Stochastic Modeling and Integration of Plug-In Hybrid Electric Vehicles in Reconfigurable Microgrids With Deep Learning-Based Forecasting

Morteza Dabbaghjamanesh, *Senior Member, IEEE*, Abdollah Kavousi-Fard, *Senior Member, IEEE*, and Jie Zhang, *Senior Member, IEEE*

***Abstract*— This paper investigates the impact of uncoordinated, coordinated, and smart charging of plug-in hybrid electric vehicles (PHEVs) on the optimal operation of microgrids (MGs) incorporating the dynamic line rating (DLR) security constraint. The DLR constraint, particularly in the islanding mode, influences the ampacity of MG feeders, when distribution lines reach their maximum capacity. To overcome any line outage or contingency situation, smart PHEVs are utilized to help improve the grid security. However, using PHEVs can cause higher power losses and feeder overloading issues. To address these concerns, a reconfiguration technique is employed in this paper. A heuristic algorithm, known as the collective decision-based optimization algorithm, is utilized to overcome the non-convexity and nonlinearity of the problem. The unscented transform technique is employed to model DLR uncertainties caused by solar radiation, load demand, and weather temperature, as well as PHEVs' uncertainties caused by varying charging strategies, numbers of PHEVs being charged, charging start time, and charging duration. Moreover, a deep learning gated recurrent unit technique is designed to forecast renewable power output for mitigating the uncertainties in renewable energy components. A modified IEEE 33-bus test network is deployed to evaluate the efficiency and performance of the proposed model.**

***Index Terms*— Smart plug-in hybrid electric vehicle, PHEV charging management, deep learning, reconfiguration.**

NOMENCLATURE

A. Sets/Indices

—,—	Index of minimum and maximum values.
$\Omega^{DL}/lm, mn, z$	Set/indices of lines.
Ω^{N}/i	Set/index of generation units.
Ω^{T}/t	Set/index of time.
λ	Index of piecewise linearization segments.

B. Constants

A'	Projected area of conductor (m^2/Linear m).
D_0	Conductor diameter.
Hc, Zc, Zl	Altitude of sun, Azimuth of sun, Azimuth of line.
I_{base}	Base value of current.
K_f	Thermal conductivity at air temperature.
mC_p	Conductor overall heat capacity (J/m-°c).
R_{mn}, X_{mn}, Z_{mn}	Resistance, reactance, impedance of distribution lines.
RU_i^G, RD_i^G	Ramp up/down rate of DG units.
T(ave)	Average temperature of aluminum strand layers (°c).
UT_i^G, DT_i^G	Minimum up/down time of DG units.
CT^S, DT^S	Energy storage minimum charging and discharging time.
δ	Time period (1 hour).
η^{Ch}, η^{Disch}	Charging/discharging efficiency.
ρ_i^G	Generation cost of the i^{th} DG unit.
ρ_t^M	Market price.
Λ	Number of segments of piecewise linear curve.
ρ_f	Air density.
ε	Emissivity.
β	Angle between the wind direction and the conductor axis.
φ	Effective angle of incidence of the sun's rays.
α	Solar absorptivity (0.23 to 0.91).
μ_f	Dynamic viscosity of air temperature.

C. Variables

C^S	Energy stored in energy storage units.
$I_{mn,t}^L$	Current flow of distribution lines.
K_{angle}	Wind direction factor.
P^{Ch}, P^{Disch}	Charging/discharging power.
P^D, Q^D	Active/reactive power demand.
$P_{mn,t}^L, Q_{mn,t}^L$	Active/reactive power flow of distribution lines.

Manuscript received November 15, 2019; revised December 28, 2019 and January 25, 2020; accepted February 10, 2020. Date of publication March 6, 2020; date of current version July 12, 2021. The Associate Editor for this article was A. Jolfaei. *(Corresponding author: Morteza Dabbaghjamanesh.)*

Morteza Dabbaghjamanesh and Jie Zhang are with the Department of Mechanical Engineering, The University of Texas at Dallas, Richardson, TX 75080 USA (e-mail: mortezadabba@utdallas.edu; jiezhang@utdallas.edu).

Abdollah Kavousi-Fard is with the Department of Electrical and Electronics Engineering, Shiraz University of Technology, Shiraz 71557, Iran (e-mail: kavousi@sutech.ac.ir).

Digital Object Identifier 10.1109/TITS.2020.2973532

$P_{i,t}^{G}$, $Q_{i,t}^{G}$	Active/reactive power of DG units.
P_{t}^{M}, Q_{t}^{M}	Active/reactive power of utility grid.
q_r, q_s, q_R, q_c	Radiated heat loss, Heat gain from sun, Resistant heat gain (W/m), Convection heat loss (W/m).
T	Conductor Temperature.
T_s, T_a	Surface temperature of conductor (°c), weather temperature (°c).
T^{Ch}, T^{Disch}	Number of consecutive charging and discharging hours.
$T_{i,t}^{G-on}$, $T_{i,t}^{G-off}$	Number of consecutive on and off hours for DG units.
V	Voltage magnitude of buses.
V_w	Wind velocity.
$w_{mn,t}^{L}$	Distribution line status.
$x_{i,t}$	Commitment state of DG units.
y^{Ch}, y^{Disch}	Energy storage charging and discharging state of charge (SOC).
$\Delta V_{mn,t}$	Required variable to apply KVL.
$\theta_{mn,t}^{L}$	Fictitious current flow regarding the distribution lines.
θ^{M}	Fictitious current flow regarding the utility grid.
θ^{D}	Fictitious current flow regarding the demand.
ψ	Covariance.
μ	Mean.

I. Introduction

A MICROGRID (MG) is the aggregation of distributed energy resources (DERs) and loads in a small electricity network that operates in both off-grid (islanded) or grid-connected modes [1]. Over the last decade, MG has attracted a great deal of attention, due to its significant advantages, such as high resiliency and reliability, low operation and planning cost, self-healing ability, and low losses within the network [2]–[6]. However, challenges still exist in MG operations, e.g., stability, scheduling, maintenance, and malfunctions still need more efforts to get solved [7]–[9].

One of the important tasks in MG is energy management for both islanded and grid-connected modes, which has been widely investigated in the literature. For example, in [10], the energy management of a MG is studied given that the MG participates in the market and competes with distribution market operators. In [11], storage units are considered in MG energy management to compensate for uncertainties associated with renewable energy resources. In [12], the energy management of a MG is investigated, considering both electric vehicles (EVs) and renewable energy resources. Li *et al.* [13] investigate the energy management of multi-agent MGs for both islanded and grid-connected operations, by utilizing an iterative bi-level optimization technique. In [14], robust optimization is employed to minimize the operation and maintenance costs simultaneously of a MG, considering an energy storage system, a wind plant, and a solar plant. In [15], the coordination of plug-in hybrid electric vehicles (PHEVs) and a MG is studied, where the main objective is to minimize the load variance. In [16], a two-stage optimization framework is developed to minimize the energy loss of a MG along with different penetration levels for PHEVs.

Although MG challenges have been explored from varied aspects, the impact of DLR on a reconfigurable MG (RMG) has yet been studied in the literature, especially with PHEVs integrated with the RMG. Technically, DLR is a practical security limitation for the ampacity of feeders, which limits the lines from approaching its maximum capacity particularly in the summer. The IEEE standard-738 requires that the heat balance equation (HBE) of the conductor depends on the conductor specifications (e.g., current, resistance, and size) and weather condition [17]. It is worth noting that comparing to bulk power networks, distribution lines of a MG are more disposed to overloading and voltage fluctuation due to higher Thevenin impedances. These can be significant issues, especially in the attendance of renewable energy and in the islanded mode, when MG lines work near their maximum capacities. To this end, to prevent any contingency and feeder overloading, considering the DLR as an independent constraint is essential.

In addition to the DLR constraint, high penetrations of uncoordinated, coordinated, and smart PHEVs are also investigated in MG operations. Therefore, this paper for the first paper investigates the optimal operation of RMGs under uncoordinated, coordinated, and smart charging schemes of PHEVs along with DLR constraints. To prevent feeder overloading and also reduce power losses within the MG network, reconfiguration is employed as a strategic technique in the grid. Reconfiguration improves the voltage profile, load balance, grid reliability and reduces the emission and line losses by changing the topology of the network through some prelocated tie switches [18], [19].

Modeling the RMG, PHEVs, and DLR constraint simultaneously will lead to a complex optimization problem with many uncertain parameters. Thus, a newly stochastic framework based on the unscented transform (UT) [20] is employed to model the uncertainties. Moreover, a deep learning gated recurrent unit (GRU) architecture is adopted to forecast hourly load demand and renewable energy output power. Also, the DLR constraint introduces a set of nonlinear equations into the RMG problem. On the other hand, due to the effect of DLR on both active and reactive power flow, AC power flow should be used, which contains nonlinear equations. To deal with the nonlinearity of the problem, a heuristic algorithm, i.e., the collective decision-based optimization algorithm (CDOA), is utilized to overcome the non-convexity and nonlinearity of the problem. Briefly, key contributions of this paper include:

- Investigation of coordinated, uncoordinated, and smart PHEVs impacts on MG operations under the DLR constraint.
- Propose a new stochastic framework based on UT to model uncertainties in PHEVs, e.g., the charging strategy and number of PHEVs to be charged.

The rest of this paper is organized as follows: Section II describes the dynamic line rating constraint. Section III presents mathematical formulations of the proposed reconfigurable MG. Section IV explains the charging behavior of PHEVs. Section V presents the stochastic UT method. Section VI presents the simulation results, followed by the conclusion in Section VII.

II. Constraint of Dynamic Thermal Line Rating

Dynamic line rating (DLR) is a practical constraint that plays a major role in the security and operation of an islanded MG, when the line current approaches its maximum capacity, especially in the summer season. The conductor temperature depends on the feeder ambient conditions, conductor current, conductor size, and resistance according to the IEEE standard 738 [17]. Indeed, the total conductor temperature is the sum of heat gains (solar and resistant heats) and the heat losses (radiated and convective heats). To this end, the HBE of the conductor at any time interval is calculated as follows [17]:

$$q_{c,z,t} + q_{r,z,t} + mCp\frac{\Delta T_{s,z,t}}{\Delta t} = q_{s,z,t} + I^2.R(T_{s,z,t}) \quad (1)$$

These terms can be defined as follows:

A. Heat Loss

The conductor heat losses are known as the convection and radiated heat losses.

1) Convective Heat Loss: Convection heat loss is classified as:

a) Natural convection: The conductor can be cooled by the surrounding air (no wind) as below:

$$q_{cn,z,t} = 3.645.\rho_f^{0.5}.D_0^{0.75}.(T_{s,z,t} - T_{a,z,t})^{1.25} \quad (w/m) \quad (2)$$

b) Forced convection: In this case, a cylinder moves the air to cool down the conductor. The forced convection, based on the IEEE standard [17], can be defined for high and low wind speeds as

$$q_{c1,z,t} = K_{angle}.[1.01 + 1.35N_{\mathrm{Re}}^{0.52}.K_f.(T_{s,z,t} - T_{a,z,t}) \quad (w/m) \quad (3)$$

$$q_{c2,z,t} = K_{angle}.0.754.N_{\mathrm{Re}}^{0.6}.K_f.(T_{s,z,t} - T_{a,z,t}) \quad (w/m) \quad (4)$$

where N_{Re} is the Reynolds number and defined as follows:

$$N_{\mathrm{Re}} = \frac{D_0.\rho_f.V_w}{\mu_f} \quad (5)$$

Moreover, K_{angle} is the wind direction and defined as

$$K_{angle} = 1.194\text{-}\cos(\beta) + 0.194cos(2\beta) + 0.3sin(2\beta) \quad (6)$$

The IEEE standard recommends that the largest value among the convection heat must be taken into consideration as:

$$q_{c,z,t} = max(q_{cn,z,t}, q_{c1,z,t}, q_{c2,z,t}) \quad (7)$$

2) Radiated Heat Loss: the conductor radiated heat can be taken into account as:

$$q_{r,z,t} = 17.8 \times D_0 \times \varepsilon \times \left(\left[\frac{T_{s,z,t}+273}{100}\right]^4 - \left[\frac{T_{a,z,t}-273}{100}\right]^4\right) \quad (w/m) \quad (8)$$

B. Heat Gain

The conductor heat gains are known as solar and resistive heat gains.

1) Solar Heat Gain: The rate of solar heat delivered by the conductor is calculated as:

$$q_{s,z,t} = \alpha.Q_{se}.\sin(\varphi).A' \quad (w/m) \quad (9)$$

$$\varphi = \arccos[\cos(H_c).\cos(Z_c - Z_l)] \quad (10)$$

2) Resistive Heat Gain: the resistive heat is obtained as:

$$q_{R,z,t} = I_{z,t}^2.R(T_{s,z,t}).I_{base} \quad (11)$$

According to (2), an approximate relationship between two time steps for the line average temperature can be assumed as:

$$T_{z,t+1} - T_{z,t} = \frac{\Delta t}{mC_p}[I^2.R(T_{s,z,t}) + q_{s,z,t} - q_{c,z,t} - q_{r,z,t}] \quad (12)$$

III. Reconfigurable MG Scheduling Formulation

The objective is to minimize the total operation costs of the MG as formulated in (13). In (13), the first term represents the cost of power exchange with the utility grid; the second term is generation costs of dispatchable generators (DGs); the third term represents the cost of power losses in distribution lines or tie lines.

$$min \sum_{t\in\Omega^T} \rho_t^M P_t^M \delta + \sum_{t\in\Omega^T} \rho_i^G P_{i,t}^G \delta + \sum_{t\in\Omega^T} \rho_t^M R_{mn} \left(I_{mn,t}^L\right)^2 \delta \quad (13)$$

The constraints of the proposed problem are categorized in three main groups.

A. Power Flow Equations

Equations (14)-(17) model the AC power flow in a radial distribution network. Indeed, the active and reactive power balances at system buses are guaranteed in constraints (14) and (15), respectively.

$$\sum_{lm\in\Omega^{DL}} \left[P_{lm,t}^L - R_{lm}\left(I_{lm,t}^L\right)^2\right] - \sum_{mn\in\Omega^{DL}} P_{mn,t}^L + P_{i,t}^G - P_t^{Ch} + P_t^{Disch} + P_t^M = P_t^D \quad \forall i \in \Omega^N, \ \forall t \in \Omega^T \quad (14)$$

$$\sum_{lm\in\Omega^{DL}} \left[Q_{lm,t}^L - X_{lm}\left(I_{lm,t}^L\right)^2\right] - \sum_{mn\in\Omega^{DL}} Q_{mn,t}^L + Q_{i,t}^G + Q_t^M = Q_t^D \quad \forall i \in \Omega^N, \ \forall t \in \Omega^T \quad (15)$$

Also, limitations (16) and (17) apply the Kirchhoff's voltage law to distribution/tie lines.

$$\left(V_{m,t}\right)^2 - \left(V_{n,t}\right)^2 = 2\left(R_{mn}P_{mn,t}^L + X_{mn}Q_{mn,t}^L\right) - (Z_{mn})^2\left(I_{mn,t}^L\right)^2 + \Delta V_{mn,t} \quad \forall mn \in \Omega^{DL}, \quad \forall t \in \Omega^T \quad (16)$$

$$\left(V_{m,t}\right)^2\left(I_{mn,t}^L\right)^2 = \left(P_{mn,t}^L\right)^2 + \left(Q_{mn,t}^L\right)^2 \quad \forall mn \in \Omega^{DL}, \ \forall t \in \Omega^T \quad (17)$$

The term $\Delta V_{mn,t}$ in (16) is an auxiliary variable. Thus, it can be positive/negative based on the difference between voltages of the sending and receiving ends of line *mn*, and can be zero when line *mn* is switched on at time t.

B. Operational Limits

The magnitude of the voltage at each bus should be within limits as (18).

$$\underline{V} \le V_{n,t} \le \overline{V} \quad \forall t \in \Omega^T,\ \forall n \in \Omega^{DL} \tag{18}$$

The current flow of distribution and tie lines should be within limits as (19). Constraint (19) also proves that the current flow of a distribution line equals to zero when it is not operating. If a distribution line is operating, the binary decision variable $w^L_{mn,t}$ is equal to one; otherwise, it is zero. Moreover, constraint (20) sets appropriate bounds on the variable $\Delta V_{mn,t}$.

$$0 \le I^L_{mn,t} \le \overline{I^L} w^L_{mn,t} \quad \forall mn \in \Omega^{DL},\ \forall t \in \Omega^T \tag{19}$$

$$\left|\Delta V_{mn,t}\right| \le \left(\overline{V} - \underline{V}\right)\left(1 - w^L_{mn,t}\right) \quad \forall mn \in \Omega^{DL},\ \forall t \in \Omega^T \tag{20}$$

The exchange of active and reactive power with the utility grid should be within limits as (21) and (22), respectively.

$$-\overline{P^M} \le P^M_t \le \overline{P^M} \quad \forall t \in \Omega^T \tag{21}$$

$$-\overline{Q^M} \le Q^M_t \le \overline{Q^M} \quad \forall t \in \Omega^T \tag{22}$$

Generation units have individual constraints for restricting active and reactive power as (23)-(24), ramp up/down (25)-(26), and min up/down time (27)-(28).

$$\underline{P^G_i} x_{i,t} \le P^G_{i,t} \le \overline{P^G_i} x_{i,t} \quad \forall t \in \Omega^T,\ \forall i \in \Omega^N \tag{23}$$

$$\underline{Q^G_i} x_{i,t} \le Q^G_{i,t} \le \overline{Q^G_i} x_{i,t} \quad \forall t \in \Omega^T,\ \forall i \in \Omega^N \tag{24}$$

$$P^G_{i,t} - P^G_{i,t-1} \le RU^G_i \quad \forall t \in \Omega^T,\ \forall i \in \Omega^N \tag{25}$$

$$P^G_{i,t-1} - P^G_{i,t} \le RD^G_i \quad \forall t \in \Omega^T \tag{26}$$

$$T^{G-on}_{i,t} \ge UT^G_i \left(x^G_{i,} - x^G_{i,t-1}\right) \quad \forall t \in \Omega^T \tag{27}$$

$$T^{G-off}_{i,t} \ge DT^G_i \left(x^G_{i,t-1} - x^G_{i,t}\right) \quad \forall t \in \Omega^T,\ \forall i \in \Omega^N \tag{28}$$

The minimum and maximum limits of charging and discharging power of energy storage are taken into account as (29) and (30), respectively.

$$\underline{P^{Ch}} y^{Ch}_t \le P^{Ch}_t \le \overline{P^{Ch}} y^{Ch}_t \quad \forall t \in \Omega^T \tag{29}$$

$$\underline{P^{Disch}_m} y^{Disch}_t \le P^{Disch}_t \le \overline{P^{Disch}} y^{Disch}_t \quad \forall t \in \Omega^T \tag{30}$$

The capacity of energy storage at any time are within limits as (31)-(32).

$$C^S_t = C^S_{t-1} - P^{Disch}_t \delta / \eta^{Disch} + P^{Ch}_t \delta \eta^{Ch} \quad \forall t \in \Omega^T \tag{31}$$

$$\underline{C^S} \le C^S_t \le \overline{C^S} \quad \forall t \in \Omega^T \tag{32}$$

Moreover, minimum charging and discharging time constraints are determined by (33) and (34), respectively.

$$T^{Ch}_t \ge CT^S \left(y^{Ch}_t - y^{Ch}_{t-1}\right) \quad \forall t \in \Omega^T \tag{33}$$

$$T^{Disch}_t \ge DT^S \left(y^{Disch}_t - y^{Disch}_{t-1}\right) \quad \forall t \in \Omega^T \tag{34}$$

The operation modes of the energy storage unit at any time are modeled by (35).

$$y^{Ch}_t + y^{Disch}_t \le 1 \quad \forall t \in \Omega^T \tag{35}$$

The DLR constraint is taken into account as (36)-(37) and assures the bounded temperature of each distribution line.

$$\left|Q^L_{nmt}\right|^2 + \left|P^L_{nmt}\right|^2 = \left|I^L_{nmt}\right|^2 . |V_{nmt}|^2 \quad \forall mn \in \Omega^{DL},\ \forall t \in \Omega^T \tag{36}$$

$$T_{nm,t} \le T_{\max} \quad \forall mn \in \Omega^{DL},\ \forall t \in \Omega^T \tag{37}$$

C. Radiality Limits

Constraints (38)-(41) assure the radiality of the network. It is worth noting that to prevent the presence of areas exclusively supplied by DGs/energy storage units, a set of fictitious current flow, denoted by θ, is provided.

$$\sum_{lm \in \Omega^{DL}} w^L_{lm,t} = 1 \quad \forall t \in \Omega^T \tag{38}$$

$$\sum_{lm \in \Omega^{DL}} \theta^L_{lm,t} - \sum_{mn \in \Omega^{DL}} \theta^L_{mn,t} + \theta^M_t = \theta^D_{i,t} \quad \forall t \in \Omega^T \tag{39}$$

$$0 \le \theta^L_{mn,t} \le \left|\Omega^N\right| w^L_{mn,t} \quad \forall mn \in \Omega^{DL},\ \forall t \in \Omega^T \tag{40}$$

$$0 \le \theta^M_t \le \left|\Omega^N\right| \quad \forall t \in \Omega^T \tag{41}$$

IV. Charging Behavior of Plug-in Hybrid Electric Vehicles

Uncertain parameters such as the charging value, number of charged PHEVs, battery capacity, charging duration and start time, and battery state of charge (SOC), have a great impact on the behavior of PHEVs. In this paper, three different scenarios of PHEVs' charging schemes are studied as follows.

A. Uncoordinated Charging

In this scenario, we assume that PHEVs leave their home in the morning and return in the evening. As a result, most of PHEVs are plugged in and start charging after arriving home, which is around 6:00 P.M. A probability distribution function (PDF) with a uniformly distributed feature to model this scenario is defined as [22]:

$$f(t_s) = \frac{1}{b-a} a \le t_s \le b \quad a = 18,\ b = 19 \tag{42}$$

B. Coordinated Charging

In this scenario, PHEVs are scheduled to charge during off-peak hours. Specifically, the charging time is postponed after 9.00 P.M, where the market price is low. Therefore, the PDF of this scenario is defined as follows.

$$f(t_s) = \frac{1}{b-a} a \le t_s \le b \quad a = 21,\ b = 24 \tag{43}$$

TABLE I
DIFFERENT TYPES OF PHEV CHARGER

Charge type	Input voltage	Maximum power (kW)
Level 1	120 VAC	1.44
Level 2	208-240 VAC	11.5
Level 3	1208-240 VAC	96
Level 3 (DC)	208-600 VDC	240

TABLE II
DIFFERENT PHEV CLASSES

Class	Market share	Min-Max C_{BT}(kWh)
Micro car	0.2	8-12
Economy car	0.3	10-14
Mid-size car	0.3	14-18
Light truck/SUV	0.3	19-23

C. Smart Charging

In this scenario, the vehicle starts charging when there is over generation capacity available, and the electricity price is low. In fact, in this scenario, the vehicle is charged when there exists a mutual interest between PHEV owners and utilities. The PDF is defined as:

$$f(t_s) = \frac{1}{\psi\sqrt{2\pi}} e^{(-\frac{1}{2}(\frac{t_S-\mu}{\sigma})^2)}, \quad \mu = 1,\ \psi = 3 \tag{44}$$

The vehicle battery is getting charged once it is connected to the charger at home. The PDF of the daily driven miles of the vehicle is modeled as:

$$f(m) = \frac{1}{m\psi\sqrt{2\pi}} e^{\frac{-(\ln(m)-\mu)^2}{2\psi^2}}, \quad m \succ 0 \tag{45}$$

The battery SOC depends on the vehicle's daily driven miles and its all-electric ranges (AER), given by [22]:

$$SOC = \begin{cases} 0 & m \succ AER \\ \dfrac{AER - m}{AER} \times 100\% & m \leq AER \end{cases} \tag{46}$$

The PHEV charging duration is then formulated as:

$$t_D = \frac{C_{BT} \times (1 - SOC) \times DOD}{\eta \times J} \tag{47}$$

Table I summarizes charging rates that depend on the charging level of chargers [22]. As can be seen, charging levels 1 and 2 are considered for home charging PHEVs. Please note that both the AC and DC charging level 3 are not considered in this study due to their main applications in public transportation. Furthermore, in this study PHEVs are divided into four classifications with different market shares and characteristics, as summarized in Table II.

The market share is modeled as a discrete distribution. Hence, PHEVs are randomly selected according to their market shares. In this study, a normal distribution is assumed as the distribution of C_{BT}.

$$\mu\ C_{BT} = \frac{Min\ C_{BT} + Max\ C_{BT}}{2} \tag{48}$$

$$\psi\ C_{BT} = \frac{Max\ C_{BT} - Min\ C_{BT}}{4} \tag{49}$$

V. STOCHASTIC OPTIMIZATION FRAMEWORK

A. Stochastic Unscented Transformer (UT) Framework

UT is a powerful and efficient uncertainty modeling method [20] with a high speed of convergence and nonlinearity handling capability, compared to conventional methods such as analytical methods (which are not suitable for nonlinear problems) and the Monte Carlo method (which needs a great number of runs to converge). Hence, the UT method is adopted in this paper to model the uncertainties associated with the proposed problem. In the UT method, it is assumed that the nonlinear problem $y = f(x)$ has h random input variables, with mean values μ and a covariance matrix ψ_x. Consequently, the output mean μ_y with convenience ψ_y is calculated by following 4 main steps.

- *Take 2h+1 samples from the uncertain input data:*

$$x_0 = \mu \tag{50}$$

$$x_\omega = \mu + (\sqrt{\frac{h}{1 - W^0}\psi_x}), \quad \omega = 1, 2, \ldots, h \tag{51}$$

$$x_\omega = \mu - (\sqrt{\frac{h}{1 - W^0}\psi_x}), \quad \omega = 1, 2, \ldots, h \tag{52}$$

Based on the assumption, W^0 is the weight of the mean value μ.

- *Calculate weighting factors of sampling points:*

$$W^0 = W^0 \tag{53}$$

$$W_\omega = \frac{1 - W^0}{2h}; \quad \omega = q + 1, \ldots, h \tag{54}$$

$$W_{\omega+q} = \frac{1 - W^0}{2h}; \quad \omega + h = h + 1, \ldots, 2h \tag{55}$$

$$\sum_{\omega \in s} W_\omega = 1 \tag{56}$$

- *Input sample points to the nonlinear function:*

$$y_\omega = f(X_\omega) \tag{57}$$

- *Calculate the output covariance ψ_y and mean μ_y of the variable Y:*

$$\mu_y = \sum_\omega W_\omega Y_\omega \tag{58}$$

$$\psi_y = \sum_\omega W_\omega (Y_\omega - \mu_y) - (Y_\omega - \mu_y)^T \tag{59}$$

As mentioned before, the formulated problem is a nonlinear and non-convex problem. Thus, the CDOA heuristic algorithm is adopted to solve the problem.

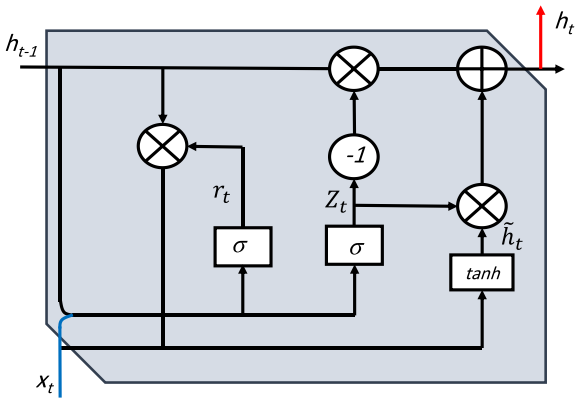

Fig. 1. Block diagram of the gated recurrent unit (GRU).

Algorithm 1 Pseudocode of the Gated Recurrent Unit

Procedure Output (h_t)
For time =1: ***horizon do***
for t =1: |***GRU|cells do***
1. $z_t \leftarrow \sigma(U_z h_{t-1} + W_z x_t + b_z)$
2. $r_t \leftarrow \sigma(U_r h_{t-1} + W_r x_t + b_r)$
3. $\tilde{h}_t \leftarrow \tanh(U(r_t \Theta h_{t-1}) W x_t$
4. $h_t \leftarrow (1 - z_t) h_{t-1} + z_t \tilde{h}_t$

end for
end for

B. Deep Learning Gated Recurrent Unit (GRU)

GRU was designed to reduce the complex structure of the long-short term memory (LSTM) [23]. Similar to LSTM, GRU includes two gated as shown in Fig. 1, which are responsible to control the flow of data from the input to the output. Based on the figure, the activation h_t at time t is a function of the candidate activation $\tilde{h}_t$ and the previous activation h_{t-1} as:

$$h_t = (1 - z_t) h_{t-1} + z_t \tilde{h}_t \tag{60}$$

where z_t is considered as the update gate, which adopts the updates of the unit for its activation or content, and is calculated as:

$$z_t = \sigma(U_z h_{t-1} + W_z x_t + b_z) \tag{61}$$

where σ is considered as a smooth parameter. Also, the differentiable activation functions W_z and U_z are considered as the input and previous activation constants of the update gate z, respectively. Moreover, b_z is the bias of the update gate z. Therefore, the candidate activation in (60) is calculated as:

$$\tilde{h}_t = \tanh(U(r_t \Theta h_{t-1}) W x_t \tag{62}$$

where Θ is an element-wise multiplication. Also, the reset gate r_t is updated as:

$$r_t = \sigma(U_r h_{t-1} + W_r x_t + b_r) \tag{63}$$

Algorithm 1 shows the pseudocode of GRU to forecast the renewable energy power output.

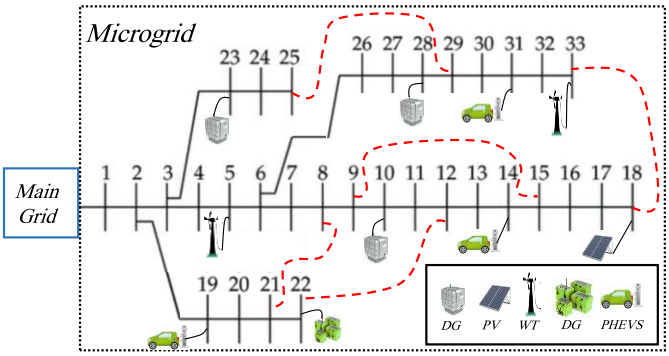

Fig. 2. Single line diagram of the tested reconfigurable MG (RMG).

TABLE III
CHARACTERISTICS OF THE ENERGY STORAGE SYSTEM

Storage	Capacity (kWh)	Min-Max Charging/Discharging Power (kW)	Min Charging/Discharging Time (h)
ESS	2,000	50-200	5

TABLE IV
CHARACTERISTICS OF DGs

Type	Min-Max Capacity (kW)	Cost ($/kWh)	Minimum/maximum of power generation rate	Min Up Time (h)
DG1	500-1,000	1.97	1,500	2
DG2	400-1,200	2.2	1,000	2
DD3	100-2,500	2.45	1,000	2

VI. SIMULATION RESULTS

A. Test System

In order to validate the performance of the proposed model, the modified IEEE 33-bus test network is selected and tested. Fig. 2 shows the single line diagram of the selected network, which is equipped with five tie switches (red dotted lines) and 33 sectionalizing switches (solid lines). The network includes three DGs (diesel generators), two wind turbines (WTs), one energy storage system, three PHEV charging stations, and one photovoltaic (PV) system. The features of energy storage and DGs are summarzied in Tables III and IV, respectively. Table V presents normalized forecasted values of hourly WTs generation, load, market price, PV generation, and temperature [24]. In addition, the required power demand of uncoordinated, coordinated, and smart PHEVs in the day-ahead horizon is depicted in Fig. 3.

B. Simulation Results

In order to evaluate the effectiveness of the proposed method, the following three cases are defined and studied.

1) Case 1: Considering the DLR Constraint in Grid-Connected Mode: In this case, the MG works in the grid-connected mode; in other words, it can exchange

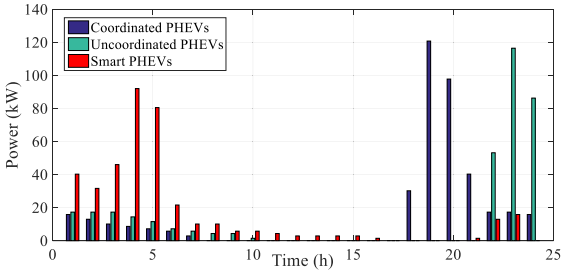

Fig. 3. Day-ahead required power of uncoordinated (a), coordinated (b), and smart (c) PHEVs.

TABLE V
HOURLY NORMALIZED FORECASTED VALUES

Hour			**1-6**			
WT power	0.119	0.119	0.119	0.119	0.119	0.061
Load (pu)	0.800	0.805	0.810	0.818	0.830	0.91
Market ($)	0.230	0.190	0.140	0.120	0.120	0.130
PV power (pu)	0.000	0.000	0.000	0.000	0.000	0.000
Tempreture	0.860	0.850	0.850	0.850	0.840	0.850
Hour			**7-12**			
WT power	0.119	0.087	0.119	0.206	0.385	0.394
Load (pu)	0.950	0.970	1.00	0.980	1.00	0.970
Market ($)	0.130	0.140	0.170	0.220	0.220	0.220
PV power (pu)	0.000	0.008	0.150	0.301	0.418	0.478
Tempreture	0.850	0.850	0.870	0.910	0.910	0.920
Hour			**13-18**			
WT power	0.261	0.158	0.119	0.087	0.119	0.119
Load (pu)	0.950	0.900	0.905	0.910	0.930	0.900
Market ($)	0.210	0.220	0.190	0.180	0.170	0.230
PV power (pu)	0.556	0.542	0.315	0.169	0.022	0.000
Tempreture	0.960	0.980	0.970	1.000	0.980	0.990
Hour			**19-24**			
WT power	0.087	0.119	0.087	0.087	0.061	0.041
Load (pu)	0.940	0.970	1.000	0.930	0.900	0.940
Market ($)	0.210	0.220	0.180	0.170	0.130	0.120
PV power (pu)	0.000	0.000	0.000	0.000	0.000	0.000
Tempreture	0.980	0.840	0.830	0.840	0.860	0.840

TABLE VI
TOTAL OPERATION COST FOR DIFFERENT CASES

Case	Operation cost ($)		
	Uncoordinated PHEV	Coordinated PHEV	Smart PHEV
Case 1	316,680.04	312,092.25	307,876.26
Case 2	317,944.82	313,442.78	309,225.68
Case 3	318,876.69	315,390.44	311,593.90

power with the utility. The output power of DGs within the MG under the coordinated, uncoordinated, and smart charging schemes of PHEVs is illustrated in Fig. 4. Based on the figure, for all types of PHEVs, DG1 and DG2, which are the cheapest units (see Table IV) generate more power than DG3. That means the output power of DGs is only based on

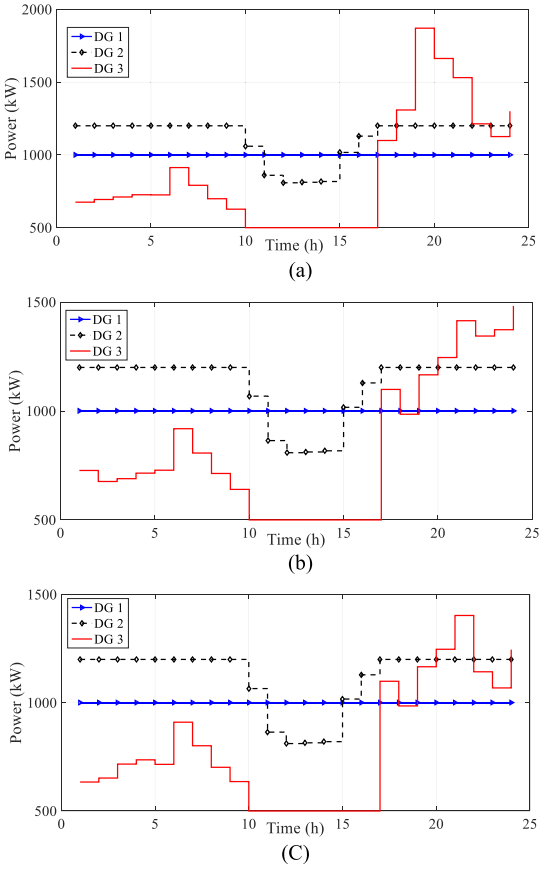

Fig. 4. DGs output power in the grid-connected mode considering the DLR constraint: (a) uncoordinated, (b) coordinated, and (c) smart PHEVs.

economic consideration. The total operation cost of the MG under the uncoordinated, coordinated, and smart charging schemes are summarized in Table VI. It is observed that the operation cost of the smart PHEV scenario is less than that of others. This is mainly because, unlike uncoordinated and coordinated PHEVs, the smart PHEV power demand is increased when the market price is decreased. For instance, at hour 6 when the market price is very low, the power demands of PHEVs with smart charging are increased (see Table VI and Fig. 4). In contrast, for coordinated PHEVs, at hour 19, the power demand is increased, when the market price is low (see Table VI and Fig. 4).

2) Case 2: Ignoring the DLR Constraint in Islanded Mode: In this case, the MG is disconnected from the main grid. Hence, the DGs within the MG should satisfy the load demand of the network, considering only conventional constraints (i.e., ignoring the DLR constraint). Fig. 5 presents the output power of the DGs in the islanded mode. Same as the previous case, the DGs output power is only based on economic consideration; that means the cheapest units are committed more than others. Similar to the previous case, the operation cost of smart charging PHEV is less than that of others. It should be noted that the operation cost of the islanded mode, for all types of PHEVs, is more than that of the grid-connected mode. These additional costs are known as the islanding cost.

TABLE VII
RECONFIGURATION SWITCHING ACTION

H	Open Switching Numbers														
	Uncoordinated PHEV					Coordinated PHEV					Smart PHEV				
	Switch #					Switch #					Switch #				
	1	2	3	4	5	1	2	3	4	5	1	2	3	4	5
1	2	38	37	15	23	7	14	21	32	22	33	35	37	12	15
2	4	35	38	17	24	20	14	8	16	24	33	34	37	38	17
3	33	34	35	37	16	5	38	11	16	23	33	36	12	11	23
4	33	34	35	38	23	2	13	11	17	24	7	12	11	30	23
5	35	36	37	38	13	7	12	38	30	23	20	13	21	15	23
6	35	36	37	4	12	35	36	37	4	12	7	13	11	17	23
7	33	35	37	12	15	33	35	37	12	15	7	14	21	17	22
8	33	34	37	38	17	33	38	37	10	17	5	12	11	16	22
9	33	36	12	11	23	33	36	37	11	23	3	12	11	15	23
10	7	12	11	30	23	4	12	8	32	23	7	14	8	17	24
11	20	13	21	15	23	7	12	11	30	23	20	12	10	17	23
12	7	13	11	17	23	20	13	21	15	23	7	12	8	15	22
13	7	14	21	17	22	7	13	11	17	23	5	12	9	32	22
14	5	12	11	16	22	7	14	21	17	22	33	35	37	12	15
15	3	12	11	15	23	5	12	11	16	22	33	34	37	10	17
16	7	14	8	17	24	3	12	11	15	23	35	36	37	38	13
17	20	12	10	17	23	7	14	8	17	24	35	36	37	4	12
18	7	12	8	15	22	20	12	10	17	23	33	35	37	12	15
19	5	12	9	32	22	7	12	8	15	22	33	34	37	38	17
20	33	35	37	12	15	33	35	37	12	15	33	36	12	11	23
21	33	34	37	10	17	33	34	37	10	17	7	12	11	30	23
22	33	36	12	11	23	33	36	12	11	23	20	13	21	15	23
23	4	12	8	27	23	4	12	8	27	23	7	13	11	17	23
24	33	13	10	17	22	33	13	10	17	22	7	14	21	17	22

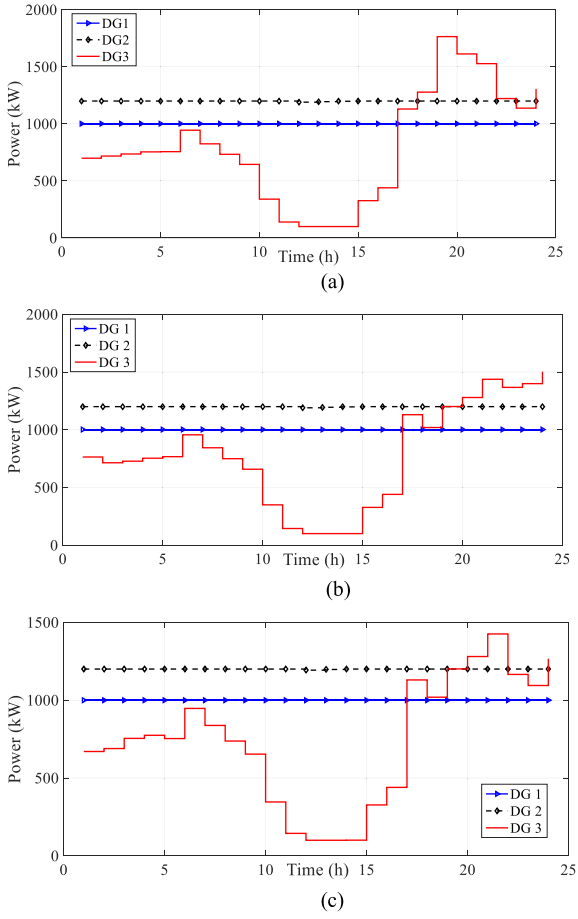

Fig. 5. DGs output power in the islanded mode ignoring the DLR constraint: (a) uncoordinated, (b) coordinated, and (c) smart PHEVs.

3) Case 3: Considering the DLR Constraint in Islanded Mode With Network Reconfiguration: In this case, the operation of the islanded MG is investigated under the effects of uncoordinated, coordinate, and smart charging of PHEVs considering the DLR security constraint. Based on simulation results, there exists a constraint violation (i.e., lines overloading) by considering the DLR constraint for uncoordinated and coordinated PHEVs. That means there is no feasible solution for the islanded MG operation. The congested lines of the uncoordinated PHEVs are L15 and L3 at the peak load hours. Also, for the coordinated charging of PHEVs, L15 is congested again at the peak load hour. To address this issue and obtain a feasible solution, a reconfiguration technique is employed. It should be noted that although the islanded MG operation under the smart PHEV has a feasible solution, the reconfiguration technique is used to decrease the power losses. Table VII presents the reconfiguration switching for MG operations considering uncoordinated, coordinated, and smart PHEVs, under the DLR limitation.

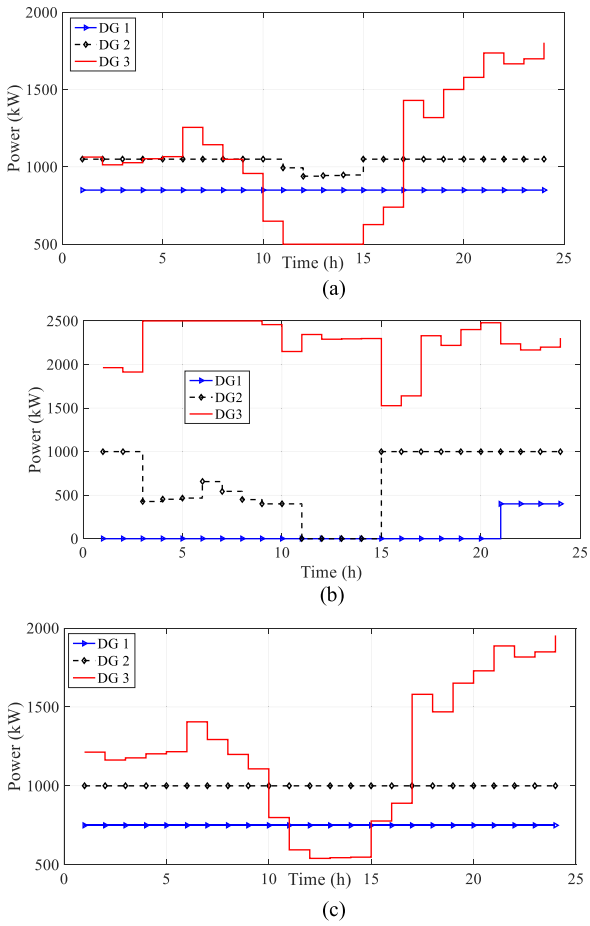

Fig. 6. DGs output power in the islanded mode considering the DLR constraint: (a) uncoordinated, (b) coordinated, and (c) smart PHEVs.

Fig. 6 depicts the optimal DGs' output power in this case after employing the reconfiguration technique. It is seen that the output power of DGs is determined not only based on economic consideration, which is also affected by the DLR constraint. For instance, unlike Cases 1 and 2, the cheapest DG (DG1) is only committed in the entire horizon by approximately 80% of its capacity. Also, in this case, due to the DLR effect, the most expensive unit (DG3) is committed more than that in Cases 1 and 2. That means, by considering the DLR constraint, the locations of DGs also affect the MG operations.

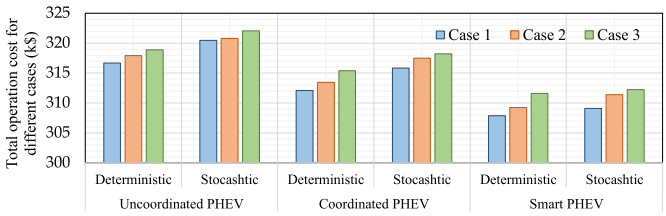

Fig. 7. Deterministic and stochastic costs for all cases (the values are based on a thousand dollars).

The total operation cost of this case is also presented in Table VI. It is worth noting that in all cases the cost of smart PHEVs is lower than that in others. Fig. 7 depicts the objective function values for both the stochastic and deterministic frameworks under different scenarios. Based on the figure, modeling the uncertainty has a significant effect on the incremental cost values across all scenarios. This additional value is the cost of having more reliable results under uncertainties.

VII. Conclusion

This paper studied the effects of DLR on the optimal power dispatch of a MG considering uncoordinated, coordinated, and smart schemes of PHEVs. We found that, by considering the DLR limitation, a feasible solution might not exist for the MG operation specially in the islanded mode. Network reconfiguration could be employed to change the topology of the network, and help obtain a feasible solution. We also found that the optimal dispatching solutions are varied when considering DRL, compared to conventional assumptions that neglect the DLR constraint to protect power lines. This is mainly due to that when conductors approach their maximum capacity in the islanded MG mode, the ampacity of the line is influenced by the DLR constraint. Potential future work will explore reconfigurable networked MGs, considering the DLR constraint. Networked MGs could be decomposed into multi interconnected MGs that can exchange power. Hence, considering the DLR constraint for both tie lines and distribution lines would be challenging. In addition, different MGs may have different weather conditions and DLR conditions, which makes the energy management more complicated.

References

[1] J. S. Giraldo, J. A. Castrillon, J. C. Lopez, M. J. Rider, and C. A. Castro, "Microgrids energy management using robust convex programming," *IEEE Trans. Smart Grid*, vol. 10, no. 4, pp. 4520–4530, Jul. 2019.

[2] M. Dabbaghjamanesh, A. Kavousi-Fard, S. Mehraeen, J. Zhang, and Z. Y. Dong, "Sensitivity analysis of renewable energy integration on stochastic energy management of automated reconfigurable hybrid AC–DC microgrid considering DLR security constraint," *IEEE Trans. Ind. Informat.*, vol. 16, no. 1, pp. 120–131, Jan. 2020.

[3] C. Ju, P. Wang, L. Goel, and Y. Xu, "A two-layer energy management system for microgrids with hybrid energy storage considering degradation costs," *IEEE Trans. Smart Grid*, vol. 9, no. 6, pp. 6047–6057, Nov. 2018.

[4] K. Rahbar, C. C. Chai, and R. Zhang, "Energy cooperation optimization in microgrids with renewable energy integration," *IEEE Trans. Smart Grid*, vol. 9, no. 2, pp. 1482–1493, Mar. 2018.

[5] A. Silani and M. J. Yazdanpanah, "Distributed optimal microgrid energy management with considering stochastic load," *IEEE Trans. Sustain. Energy*, vol. 10, no. 2, pp. 729–737, Apr. 2019.

[6] B. Wang, M. Dabbaghjamanesh, A. Kavousi-Fard, and S. Mehraeen, "Cybersecurity enhancement of power trading within the networked microgrids based on blockchain and directed acyclic graph approach," *IEEE Trans. Ind. Appl.*, vol. 55, no. 6, pp. 7300–7309, Nov. 2019.

[7] C. Liu, J. Wang, A. Botterud, Y. Zhou, and A. Vyas, "Assessment of impacts of PHEV charging patterns on wind-thermal scheduling by stochastic unit commitment," *IEEE Trans. Smart Grid*, vol. 3, no. 2, pp. 675–683, Jun. 2012.

[8] M. Dabbaghjamanesh, A. Kavousi-Fard, and S. Mehraeen, "Effective scheduling of reconfigurable microgrids with dynamic thermal line rating," *IEEE Trans. Ind. Electron.*, vol. 66, no. 2, pp. 1552–1564, Feb. 2019.

[9] H. Kim and T. Kinoshita, "A new challenge of microgrid operation," in *Proc. Int. Conf. Secur.-Enriched Urban Comput. Smart Grid* Berlin, Germany: Springer, 2010, pp. 250–260.

[10] C. Zhang, Y. Xu, and Z. Y. Dong, "Robustly coordinated operation of a multi-energy micro-grid in grid-connected and islanded modes under uncertainties," *IEEE Trans. Sustain. Energy*, to be published.

[11] M. Dabbaghjamanesh *et al.*, "A novel two-stage multi-layer constrained spectral clustering strategy for intentional islanding of power grids," *IEEE Trans. Power Del.*, to be published.

[12] Y. Guo, J. Xiong, S. Xu, and W. Su, "Two-stage economic operation of microgrid-like electric vehicle parking deck," *IEEE Trans. Smart Grid*, vol. 7, no. 3, pp. 1703–1712, May 2016.

[13] J. Li, Y. Liu, and L. Wu, "Optimal operation for community-based multi-party microgrid in grid-connected and islanded modes," *IEEE Trans. Smart Grid*, vol. 9, no. 2, pp. 756–765, Mar. 2018.

[14] C. Zhang, Y. Xu, Z. Y. Dong, and J. Ma, "Robust operation of microgrids via two-stage coordinated energy storage and direct load control," *IEEE Trans. Power Syst.*, vol. 32, no. 4, pp. 2858–2868, Jul. 2017.

[15] L. Jian, H. Xue, G. Xu, X. Zhu, D. Zhao, and Z. Y. Shao, "Regulated charging of plug-in hybrid electric vehicles for minimizing load variance in household smart microgrid," *IEEE Trans. Ind. Electron.*, vol. 60, no. 8, pp. 3218–3226, Aug. 2013.

[16] H. Nafisi, S. M. M. Agah, H. A. Abyaneh, and M. Abedi, "Two-stage optimization method for energy loss minimization in microgrid based on smart power management scheme of PHEVs," *IEEE Trans. Smart Grid*, vol. 7, no. 3, pp. 1268–1276, May 2016.

[17] *IEEE Standard for Calculating the Current-Temperature of Bare Overhead Conductors*, Standard IEEE 738-2006, 2007.

[18] M. A. Kashem, V. Ganapathy, and G. B. Jasmon, "Network reconfiguration for load balancing in distribution networks," *IEE Proc., Gener. Transm. Distrib.*, vol. 146, no. 6, pp. 563–567, 1999.

[19] F. Ferdowsi, M. Dabbaghjamanesh, S. Mehraeen, and M. Rastegar, "Optimal scheduling of reconfigurable hybrid AC/DC microgrid under DLR security constraint," in *Proc. IEEE Green Technol. Conf. (GreenTech)*, Lafayette, LA, USA, Apr. 2019, pp. 1–5.

[20] A. K. Fard, B. Wang, O. Avatefipour, M. Dabbaghjamanesh, R. Sahba, and A. Sahba, "Superconducting fault current limiter allocation in reconfigurable smart grids," in *Proc. 3rd Int. Conf. Smart Grid Smart Cities (ICSGSC)*, Berkeley, CA, USA, Jun. 2019, pp. 76–80.

[21] S. Senemar, M. Rastegar, M. Dabbaghjamanesh, and N. D. Hatziargyriou, "Dynamic structural sizing of residential energy hubs," *IEEE Trans. Sustain. Energy*, to be published.

[22] M. Dabbaghjamanesh, S. Mehraeen, A. Kavousi-Fard, and F. Ferdowsi, "A new efficient stochastic energy management technique for interconnected AC microgrids," in *Proc. IEEE Power Energy Soc. General Meeting (PESGM)*, Portland, OR, USA, Aug. 2018, pp. 1–5.

[23] J. Chung, C. Gulcehre, K. Cho, and Y. Bengio, "Empirical evaluation of gated recurrent neural networks on sequence modeling," 2014, *arXiv:1412.3555*. [Online]. Available: http://arxiv.org/abs/1412.3555

[24] M. Dabbaghjamanesh, A. Kavousi-Fard, and Z. Dong, "A novel distributed cloud-fog based framework for energy management of networked microgrids," *IEEE Trans. Power Syst.*, to be published.

Morteza Dabbaghjamanesh (Senior Member, IEEE) received the M.Sc. degree in electrical engineering from Northern Illinois University, DeKalb, IL, USA, in 2014, and the Ph.D. degree in electrical and computer engineering from Louisiana State University, Baton Rouge, LA, USA, in 2019. In 2015, he joined the Renewable Energy and Smart Grid Laboratory, Louisiana State University. In 2019, he joined the Design and Optimization of Energy Systems (DOES) Laboratory, The University of Texas at Dallas, Richardson, TX, USA. He is currently a Research Associate at The University of Texas at Dallas. His current research interests include power system operation, reliability, and resiliency, renewable energy sources, cybersecurity analysis, machine learning, smart grids, and microgrids.

Abdollah Kavousi-Fard (Senior Member, IEEE) received the B.Sc. degree from the Shiraz University of Technology, Shiraz, Iran, in 2009, the M.Sc. degree from Shiraz University, Shiraz, in 2011, and the Ph.D. degree from Shiraz University of Technology, in 2016, all in electrical engineering. He was a Postdoctoral Research Assistant at the University of Michigan, MI, USA, from 2016 to 2018. He was a Researcher with the University of Denver, Denver, CO, USA, from 2015 to 2016, conducting research on microgrids. His current research interests include operation, management and cyber security analysis of smart grids, microgrid, smart city, electric vehicles as well as protection of power systems, reliability, artificial intelligence, and machine learning. He is an Editor of *ISTE ISI Journal* (Springer).

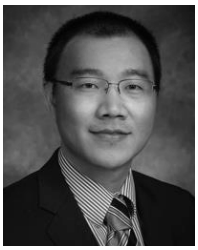

Jie Zhang (Senior Member, IEEE) received the B.S. and M.S. degrees from the Huazhong University of Science and Technology, Wuhan, China, in 2006 and 2008, respectively, and the Ph.D. degree from the Rensselaer Polytechnic Institute, Troy, NY, USA, in 2012, all in mechanical engineering. He is currently an Assistant Professor with the Department of Mechanical Engineering, The University of Texas at Dallas. His research interests include multidisciplinary design optimization, complex engineered systems, big data analytics, wind and solar forecasting, renewable integration, and energy systems modeling and simulation.